Alkali-metal negative ions. IV. Multichannel calculations of K^- photodetachment

K. T. Taylor* and D. W. Norcross†
Joint Institute for Laboratory Astrophysics, National Bureau of Standards and University of Colorado, Boulder, Colorado 80309-0440
(Received 28 April 1986)

The results of *ab initio* calculations of photodetachment of K^- are presented and compared with experimental measurements. The energy region studied is from threshold to the vicinity of the first excited state of neutral potassium. The calculations are essentially nonrelativistic in nature, but the fine structure in the first excited state (a doublet) is resolved in the calculations by a three-step process: a transformation of dynamical variables to a form that is relatively independent of energy over an energy range comparable to the splitting, an algebraic transformation from *LS* to *jj* coupling, and finally by kinematic corrections for the splitting. The initial transformation, a simple phase rotation, was determined empirically, but is shown to be consistent with a formal correction for the effects of long-range polarization forces in electron scattering by potassium near the $4p\,^2P^o$ threshold.

I. INTRODUCTION

The alkali-metal atoms have electron affinities of about half an eV; absorption of a visible photon by the negative ion can leave the atom in either the ground state or in one of the first few excited states. The excited states of the alkali-metal atoms are highly polarizable and the first excited state is a fine-structure doublet ($np\,^2P^o$). On the basis of the Wigner[1] threshold law the cross section for photodetachment near this threshold should behave as $E^{1/2}$, where E is the energy of the outgoing electron relative to threshold. This would provide an unambiguous signature of the excited-state threshold and thus a precise determination of the electron affinity.[2]

The first measurements[3] of this type for the alkali-metal negative ions (for K^-, Rb^-, and Cs^-) revealed fascinating resonance structure presumably associated with doubly excited states of the negative ions. Subsequent measurements[4] for K^- and Cs^- using a high-resolution cw dye laser probed in more detail the energy range in the vicinity of the first excited state ($4p\,^2P^o$ for potassium). While not absolute measurements, these were the first to resolve the fine structure of the doublet, and to provide an estimate of the branching ratio for production of the excited states.

Previous measurements of K^- photodetachment include low-resolution (flashlamp based), but absolute measurements[5] from the ground-state threshold to about 2.3 eV above it; and crossed ion-laser beam measurements[6] in a broad energy range around the $4p\,^2P^o$ threshold. More recent work includes measurements[7] using crossed ion-laser beams, the first to separately resolve excitation to the two fine-structure states of the excited-state doublet (for K^- and Rb^-), and to obtain precise results for the branching ratios to these states and the ground state.

Earlier calculations[8] of photodetachment cross sections for K^- employed a semiempirical model potential to represent the effects of the inner closed shells of electrons, only the outer electron being treated explicitly. The results were in very good agreement with the shape of the (relative) measured[6] cross section near the $4p\,^2P^o$ threshold, and well within the uncertainty associated with the absolute measurements[5] at lower energies. These calculations were, however, carried out completely in *LS* coupling, and thus did not allow for the fine-structure splitting of the doublet final state.

The present study was designed to make some contribution to the understanding of the observed structure near these thresholds, and near-threshold photodetachment behavior in general, for highly polarizable systems. The choice of K^- for initial study was dictated by the success of the earlier work,[8] and the fact that K^- has fewer electrons and a weaker spin-orbit interaction than either Rb^- or Cs^-. Our calculations are fundamentally nonrelativistic in nature; the fine-structure splitting is introduced after the fact of photodetachment calculations carried out in *LS* coupling, by an algebraic transformation combined with the introduction of appropriate kinematic factors.

The calculations were carried out using the University College London suite of computer codes.[9] These allow for the inclusion of the interaction of the photon and outgoing electron with *all* target electrons. Subtle effects such as core polarization can be included *ab initio,* or (as in the present work) by a semiempirical approach. As a by-product of the calculations, we obtain oscillator strengths and the electron affinity of potassium, which provide useful checks on the accuracy of the calculations.

The analysis that leads to photodetachment cross sections in *jj* coupling is based on the assumption that the essential dynamical parameters of the photodetachment process are independent of energy on the scale of the fine-structure splitting, i.e., that photodetachment is driven by an interaction that occurs at short distances where the electrons are moving rapidly, but that the energy dependence of the threshold behavior is controlled by the final-state interaction of atom and low-energy outgoing electron. This assumption is fundamental to all so-called effective range theories of scattering (see, e.g., Ross and Shaw[10]) by neutral systems and to quantum-defect theory[1] for electron-ion scattering and radiative transitions, in both of which the fundamental quantities describing the process (reactance matrices **R**, radiative

matrix elements $\vec{D}$) are determined relative to scattering wave functions with the appropriate kinematic normalization. These quantities are then relatively slowly varying as a function of energy near threshold and quasianalytic (i.e., can be extrapolated through threshold).

It is immediately recognized[3,8] that the observed resonance behavior and very rapid onset of the photodetachment cross sections near the $np\,^2P^o$ thresholds of the heavier alkali metals was likely a consequence of the highly polarizable nature of these states. This was confirmed by a reanalysis[12] of the present results for the fundamental quantities $\mathbf{R}$ and $\vec{D}$ for K^-, originally obtained relative to a basis of plane waves at infinity and found to be strongly dependent on energy. Using a straightforward transformation to a basis including the long-range polarization force at infinity, Watanabe and Green showed[12] that the resulting functions $\mathbf{R}_p$ and $\vec{D}_p$ are effectively constant, rather than rapidly varying, over the energy range of the fine-structure splitting. They concluded that "to reproduce this [the original] energy dependence qualitatively, we have found it necessary to use the full transformation" given by a complete and rigorous treatment of the long-range polarization force.

This conclusion differs from that of Lee,[13] who was able to carry out an impressive *and* predictive analysis of the photodetachment measurements[3,4] for Cs^- using a formalism that completely neglected any effect due to long-range forces, i.e., using semiempirically determined quantities $\mathbf{R}$ and $\vec{D}$ that were apparently relative to a plane-wave basis but presumed constant, or nearly so, over the energy range of the Cs^- fine-structure splitting.

In the present work we suggest an explanation for the success of Lee's analysis by showing that the photodetachment cross section (or any other inelastic process) is invariant if the fundamental quantities $\mathbf{R}$ and $\vec{D}$ are appropriately transformed by *any* unitary matrix that is diagonal in the channels resolved in the measurements. This transformation also leaves the *form* of the expressions used to calculate the measured quantities unchanged. Thus Lee's analysis led to extracted values of $\mathbf{R}$ and $\vec{D}$ that are essentially ambiguous to within any such transformation; the fact that quasiconstants were obtained implies that Lee's values are related to the usual plane-wave-based quantities by a transformation that effectively extracts the contribution from long-range polarization forces. Since a complete and rigorous treatment of the long-range polarization force does *not* leave the form of the expressions unchanged from their zero-order plane-wave-based form, this implies that such a rigorous treatment, while perhaps useful, may not always be necessary.

We demonstrate this by deducing a simple transformation for our plane-wave-based results for $\mathbf{R}$ and $\vec{D}$ for K^- photodetachment that turns them into quasiconstants, leaves the form of the expressions used to calculate the photodetachment cross sections unchanged, and reproduces the shape and branching ratios for these cross sections to quite reasonable accuracy. This transformation is obtained without any specific reference to the long-range polarization force, but is shown to be consistent with the strength of this interaction for the $4p\,^2P^o$ state of potassium.

The remainder of the paper is organized as follows. Section II contains two subsections: the first details the development of suitable wave functions for the various states of the potassium atom; the second discusses their use in describing states of the electron plus potassium complex. In Sec. III we present results for the electron affinity of potassium and for scattering and photodetachment in LS coupling. The formalism used to transform the fundamental quantities $\mathbf{R}$ and $\vec{D}$ is summarized in Sec. IV, and results for the photodetachment cross sections in jj coupling are presented and compared with measurements in Sec. V.

II. DEVELOPMENT OF WAVE FUNCTIONS

A. States of the potassium atom

The underlying idea in these calculations was to start with a wave function for the closed-shell core K^+ system and, using close-coupling expansions, to build on this frozen core further functions that represent states of the K atom and $K+e$ collision complex. A set of orbitals was first chosen so that a wave function representing the K^+ system could be formed by combining such orbitals in a Slater determinant. These orbitals were optimized variationally on the ground state of K^+, resulting in a good approximation to the Hatree-Fock energy for this closed-shell system. They were taken as adequate to describe also the inner electrons of the K atom; orbitals needed in representing the outer electron for this system were obtained as follows.

Wave functions Ψ_i for various states of the K atom were taken to have the form

$$\Psi_i = A\psi_0 F_i(r_{N+1}) , \tag{2.1}$$

where ψ_0 represents the K^+ wave function, composed as described above, coupled to the angular and spin parts of the added electron orbital. F_i represents the reduced radial part of this added orbital while A is the antisymmetrization operator. Substitution of this form of the wave function in the Schrödinger equation results in the standard second-order integrodifferential equation for F_i

$$\left[\frac{d^2}{dr^2}+\frac{l_i(l_i+1)}{r^2}-V+k^2\right]F_i=0 , \tag{2.2}$$

where l_i is the orbital angular momentum of the added electron, V is the potential operator representing the effect of the nucleus plus other electrons in the system, and k^2 is the energy (in Ry) of the added electron.

In solving (2.2) the standard static-exchange form of the potential V was augmented by a term V_p, where

$$V_p(r)=\alpha[1-\exp(-r/r_c)^6]\frac{1}{r^4} . \tag{2.3}$$

This polarization potential represents the effect on the added electron of the distortion of the closed-shell core; $\alpha=5.473$ a.u. was taken as the polarizability of the K^+ ground state.[14] The values of k^2 for which bound-state solutions to (2.2) exist was determined by varying r_c until

the lowest bound-state solution for a given symmetry was in agreement with spectroscopic measurement.[14]

In Table I we list the K states ($4s$, $4p$, and $3d$) for which wave functions were generated explicitly in this way together with corresponding values of r_c. As an indication of the quality of the chosen polarizational potential, calculated energies, and quantum defects together with those deduced from spectroscopic measurements for several higher states are also included in Table I.

Oscillator strengths for transitions among the four lowest states of K are compared with measured results in Table II. The calculated values were obtained both with and without a correction for core polarization in the dipole matrix element. This matrix element can be written in general[18] for a one-electron transition

$$\langle nl \mid \vec{r}[1-V_p(r_i,r_f)] \mid n'l' \rangle , \tag{2.4}$$

where r_i and r_f are the radial coordinates of the electrons in the initial and final states. In the present case we take

$$V_p(r_i,r_f)=[V_p(r_i)V_p(r_f)]^{1/2}r , \tag{2.5}$$

with the average of the values of r_c from Table I used in $V_p(r)$.

These wave functions for the K system were used as the basis for a close-coupling expansion of wave functions describing states of the $K+e$ complex. When wave functions representing states of the atom are to be used in this way it is important to have some estimate of the effects produced by the unavoidable omission of the infinity of other states, both bound and continuum, needed to make the expansion complete. The effects will depend on the energy of the colliding electron, but two energy regions are of particular importance in our calculations. The first is a single energy point about 0.5 eV below the ground-state energy of the K atom corresponding to capture of the electron into the stable bound state of the K^- ion. The second spans about 0.02 eV either side of the first excited state of the atom. In the first case it is the interaction with the ^2S ground atomic state, in the second, that with the $^2P^o$ excited state, that we must take particular care to represent correctly.

One of the most important interactions in the long-range polarization force between atom and incident electron, and one of the simplest measures of the accuracy and convergence of the close-coupling expansion is the fraction of the total polarizability of a particular atomic state contributed by other states included in the expansion. In Table III we compare the contribution to the polarizabilities of the $4s$ and $4p$ states from the lowest few states with the best available data for the total.

B. Close-coupling representations of the $K+e$ system

These wave functions have the form

$$\Psi_f=A\sum_i \frac{1}{r}\Theta_i F_i(r_{N+2})+\sum_j \phi_j(N+2)c_j , \tag{2.6}$$

where Θ_i represents the wave function for the atom, Ψ_i, coupled to spin and angular components of that for the added electron, while $F_i(r_{N+2})$ is the reduced radial part of the added electron orbital. The ϕ_j are antisymmetrized bound-type wave functions describing all the electrons in the system and are formed entirely from the bound orbitals included in the target representation. The c_j are energy-dependent variational coefficients.

We used three distinct close-coupling representations for each of the $^1S^e$, $^1P^o$, and $^3P^o$ symmetries of the $K+e$ collision process. These, referred to below as two, three, and four state, correspond to retaining only the $4s\,^2S^e$ and $4p\,^2P^o$ states of the atom (two state); adding next the $3d\,^2D^e$ state (three state); and finally also the $5s\,^2S^e$ state (four state). From Table III, we might expect the two-state approximation to be reasonably good at low collision energies, but the three- or four-state approximations to be required for good convergence for energies near the $4p$ state.

The scattering equations to be solved are analogous to the single equation (2.2) discussed above except that now a set of coupled equations is involved. Moreover, the potential V in the equations was chosen to include a dielectronic polarization term of the form

$$V_p(r_1,r_2)=V_p(r_1)+V_p(r_2) -2\hat{\mathbf{r}}_1\cdot\hat{\mathbf{r}}_2[V_p(r_1)V_p(r_2)]^{1/2} , \tag{2.7}$$

where r_1 and r_2 are the radial coordinates of the two electrons existing outside the closed K^+ core. The value of r_c used in this expression was taken as the average of those values used in finding the various potassium wave func-

TABLE I. Ionization energies (IP, in Ry) and effective quantum numbers (n^*) for K states; r_c is the cutoff radius in the polarization potential.

		Calculated		Measured[a]	
r_c	nl	IP	n^*	IP	n^*
2.526	$4s$	0.319 04	1.7704	0.319 04	1.7704
	$5s$	0.127 10	2.8049	0.127 43	2.8014
	$6s$	0.068 72	3.8146	0.068 88	3.8101
2.490	$4p$	0.200 36	2.2341	0.200 36	2.2341
	$5p$	0.093 75	3.2660	0.093 82	3.2647
	$6p$	0.054 68	4.2766	0.054 72	4.2749
2.774	$3d$	0.122 79	2.8538	0.122 79	2.8538
	$4d$	0.069 20	3.8015	0.069 37	3.7968
	$5d$	0.043 82	4.7772	0.043 96	4.7693

[a]Reference 14.

TABLE II. Oscillator strengths (absorption) for the target states.

Transition	Oscillator strengths Calculated		Other
$4s$-$4p$	1.087[a]	1.003[b]	1.00±0.02[c]
$4p$-$5s$	0.183	0.186	0.183[d]
$4p$-$3d$	0.856	0.823	0.81±0.05[e]

[a]Without core polarization correction.
[b]With core polarization correction.
[c]Average of six experimental values, Ref. 15.
[d]Reference 16.
[e]Reference 17.

TABLE III. Polarizabilities (in a.u.) of the $4s$ and $4p$ states of K contributed by couplings to nearby states, as a function of the total.

	Polarizabilities (a.u.) Calculated[a]	Other	Percent of total
$4s$-$4p$	290.4		98.9
$4s$ total		293±6[b]	
$4p$-$4s$	−89.5		
$4p$-$4s,3d$	457.6		$\lesssim$7.58
$4p$-$4s,3d,5s$	595.9		
$4p$ total		$\gtrsim$604.0[c]	$\lesssim$98.7

[a]Using f values that include the core polarization correction, and also the core contribution itself.
[b]Measurements of Ref. 19.
[c]Using Ref. 20 to estimate contribution from states higher than $3d$ and $5s$.

tions. The third term in (2.7), the dielectronic correction, is thus consistent with the core polarization correction (2.5) used in evaluating the oscillator strengths.

Terms representing exchange between the added electron and others of the system were neglected beyond a radial distance where the density of the most diffuse orbital included had fallen to 0.01% of its maximum value. This occurred at 37.65 a.u. for the two-state, 49.41 a.u. for the three-state, and 51.78 a.u. for the four-state calculation. Almost all previous calculations of this type for any system have been confined to a region not exceeding ~ 10 a.u. in radial dimension, and so care was taken that wave functions in the much larger interaction region involved here should be free of any numerical inadequacies or inconsistencies. To this end, the prescription for generating the radial mesh was carefully chosen. This was done by making a series of trials corresponding to different mesh choices, then for each choice solving the equations at some small positive energy relative to the atom ground state with the potential entirely neglected. With perfect numerics the reactance matrix describing the collision process would be zero in all its elements, i.e., the program should solve for uncoupled spherical Bessel functions. That mesh giving a reactance matrix closest to zero (<0.001) was taken as the optimum choice and used in all subsequent calculations.

All possible collision channels leading to the $^1S^e$, $^1P^o$, and $^3P^o$ symmetries of the $K+e$ system were retained except in treating $^1P^o$ and $^3P^o$ scattering in the three-state approach, where the $l=3$ angular momentum channel coupled to the $3d\,^2D^e$ state of the atom was neglected. In the largest cases, namely the four-state representation of the $^1P^o$ and $^3P^o$ symmetries, the inclusion of all six possible channels and an integration mesh of 93 points meant solving a set of ~ 600 simultaneous linear-algebraic equations at every energy required.

A further problem in these four-state calculations occurred in the energy region just above the $^2P^o$ threshold. At these energies the strongly closed, nearly degenerate, channels coupled to the $5s\,^2S^e$ and $3d\,^2D^e$ states caused numerical problems in the asymptotic region. An integration inward from roughly 1000 a.u., using a technique developed[21] for such problems, was required in order that the newly opened channel functions be accurately calculated.

III. RESULTS IN *LS* COUPLING

A. Electron affinity of potassium

The first quantity calculated was the electron affinity of potassium. This was done by solving the close-coupling equations in $^1S^e$ symmetry with all collision channels closed. In Table IV we present the electron-affinity values yielded by the two-, three-, and four-state

TABLE IV. Electron affinity (Ry) of potassium, and coefficients of $nln'l'$ configurations in the wave function.

	Calculated Two states[a]	Three states[a]	Four states[a]	Four states[b]	Measured[c]
E_{EA}	0.0349	0.0354	0.0362	0.0404	0.0369
Configurations					
$4s^2$	−0.9319	−0.9369	−0.8262	−0.8351	
$4p^2$	0.3627	0.3483	0.3059	0.3252	
$3d^2$		−0.0287	−0.0257	0.0188	
$5s^2$			0.0002	−0.0003	
$4s5s$			0.4723	0.4437	

[a]With the dielectronic term in Eq. (2.7).
[b]Without the dielectronic term in Eq. (2.7).
[c]Reference 4.

calculations compared with the best experimental result available. Especially pleasing is the improved agreement between calculation and experiment as the sophistication of the calculation increases, to the point where the four-state result is within less than 2% of the experimental result.

The close-coupling equations were also solved omitting the last interference term, the dielectronic polarization potential, in (2.7). We note from Table IV that the inclusion of this term lowers the electron affinity by ~ 0.06 eV, thus significantly improving the agreement with experiment.

Also set out in Table IV are the normalized coefficients [c_j of (2.6)] of configurations employing products of potassium orbitals in the expansion representation of the K^- wave functions. Particularly interesting is the large coefficient of the $4s5s$ configuration that appears in the four-state results. This makes it the most important configuration after the basic configuration $4s^2$. Two further observations are noteworthy. The magnitude of none of the coefficients changes markedly by omitting the dielectronic interference term in the four-state calculation, and the $3d^2$ and $5s^2$ configurations have very small coefficients.

B. Electron scattering

The close-coupling equations in all three approximations were solved for $^1P^o$ and $^3P^o$ symmetries over a mesh of energies from the ground-state threshold of the atom to beyond the threshold for the first excited state. The eigenphase sum, the generalization of the single-channel phase shift to the multichannel situation, is a useful measure of the results.

In Fig. 1 we present its behavior for the $^1P^o$ collision symmetry over a small important energy region about the $^2P^o$ threshold. Below this threshold where only one channel is open, the eigenphase sum is a simple phase shift. We see from the figure that this phase shift increases only slightly in the two-state calculation as the threshold is approached, but rises through almost $\pi/2$ radians in the three- and four-state calculations. We also note the increasing magnitude of the phase shift (and eigenphase sum above threshold) in going from the two- to the three- to the four-state calculations. This is in accord with the variational principle predicting a larger phase shift the greater the number of closed channels. However, the major change in the eigenphase sum (both above and below threshold) occurs in going from the two- to three-state calculation—the difference between the three- and four-state results is very small. Thus it would appear that the $^1P^o$ eigenphase sum over this energy region is converged, at least to within addition of s states of the atom, in our wave-function expansion.

As an inset in Fig. 1, we show the change with energy of the partial $^1P^o$ cross sections for elastic scattering from the first excited state and for exciting the atom from its ground to its first excited state. The former falls off very rapidly from threshold, while the latter climbs to near its maximum value in less than 2×10^{-4} Ry above threshold.

The variation with energy of the $^3P^o$ eigenphase sum is displayed over the same energy region in Fig. 2. Below the $^2P^o$ threshold the calculated phase shift appears to be converged, as it changes insignificantly in passing from the two- to three-state approximation. Above threshold the behavior is completely different. As we pass from the two- to the four-state result the inelastic s-wave eigenphase increases progressively more rapidly from zero over a range within 5×10^{-5} Ry of threshold, in contrast to the two-state result, for which this inelastic eigenphase actually decreases from zero over this energy range. (The d-wave inelastic eigenphase stays close to zero in all calculations.)

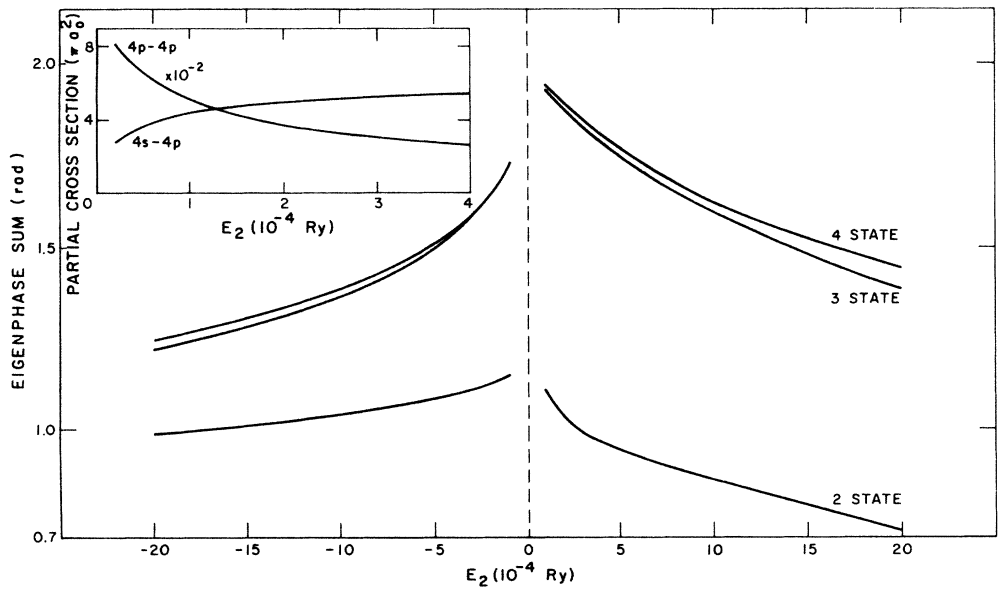

FIG. 1. Eigenphase sums for electron-potassium scattering in the $^1P^o$ partial wave near the $4p\,^2P^o$ threshold in the two-, three-, and four-state approximations, and (inset) partial cross sections for excitation ($4s$-$4p$) of and elastic scattering ($4p$-$4p$) from the excited state in the four-state approximation; the energy scale is relative to this threshold.

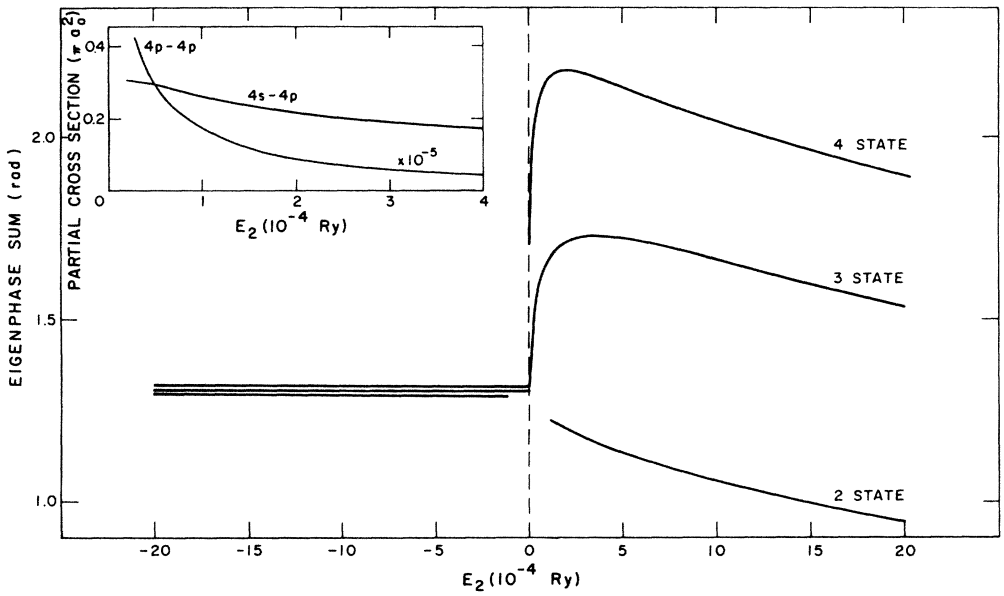

FIG. 2. As in Fig. 1 for the $^3P^o$ partial wave.

The three- and four-state results indicate the presence of a virtual state lying very close to the $^2P^o$ threshold. The lack of convergence in the eigenphase sums can be explained by the difficulty in determining precisely the position of such a virtual state so near threshold. The movement of the virtual state a fraction of a millivolt nearer threshold produces a greatly increased rate of rise of the inelastic eigenphase and hence a much larger eigenphase sum a short distance above threshold.

A virtual state closer to threshold would also imply a large threshold value for the partial $^3P^o$ cross section for elastic electron scattering from the excited $^2P^o$ state of the atom. The inset in Fig. 2 shows that the four-state calculation already yields a value of $\sim 10^5 \pi a_0^2$ for this quantity. Also shown is the inelastic electron scattering cross section for excitation of the atom from its ground state to first excited state as given by the four-state approximation. This has already increased from zero and is decreasing from its maximum value at the first calculated energy point, 2×10^{-5} Ry above threshold.

We must conclude that, in contrast to our results for $^1P^o$ symmetry, the calculated $^3P^o$ eigenphase sum above the $^2P^o$ threshold is not yet converged for addition of s states of the atom in the close-coupling expansion, perhaps not also for d states.

C. Photodetachment

Wave functions representing the bound state of the K^- ion mentioned in Sec. III A, and various free states of the $K+e$ scattering system in $^1P^o$ symmetry discussed in Sec. III B, were used in calculating the photodetachment cross section of K^-. The cross section is given by the expression

$$\sigma_f = 4\pi^2 \alpha a_0^2 \frac{h\nu}{\omega} |\langle \Psi_f^{(-)}(\hat{\mathbf{k}}) | \hat{\mathbf{n}}\cdot\hat{\mathbf{r}} | \Psi_b \rangle|^2 , \tag{3.1}$$

where Ψ_b is the wave function representing the K^- ion, $\Psi_f^{(-)}(\hat{\mathbf{k}})$ is the wave function representing the $K+e$ system after the photon absorption with the free electron having an energy k^2 at an infinite distance from the residual atom in state f, $\hat{\mathbf{n}}$ is the polarization of the incident radiation, $h\nu$ is the photon energy (in Ry), α is the fine-structure constant, ω is the statistical weight of the initial state, and a_0 is the Bohr radius.

In Fig. 3 we give the photodetachment cross section as calculated in the two- and four-state approximations over an energy range from threshold to just below the $^2P^o$ first excited state of the atom. The results are compared with the absolute measurements of Kaiser *et al.*[5] The good agreement between the two calculations over most of the energy range is satisfying, as is the fact that they both lie within the few representative error bars included on the experimental results. It is only near the $^2P^o$ threshold that any great differences become noticeable. The total [sum-

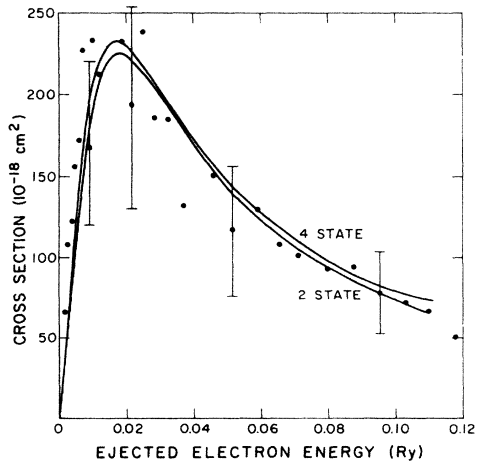

FIG. 3. Total photodetachment cross section for K^- in the two- and four-state approximations and in *LS* coupling compared with the absolute measurements of Ref. 5.

ming (3.1) over all final atomic states] cross section in this region is set out on a larger scale in Fig. 4, where some experimental results of Patterson, Hotop, and Lineberger[6] are also plotted. These measurements are not absolute but have been normalized to the results of the four-state calculation.

It is apparent that the two-state calculation yields an incorrect cross section in this region. The failure of the $^1P^o$ final-state phase shift to pass through the value of $\pi/2$ radians below threshold prevents any resonance feature appearing there. Both the three- and four-state calculations have a resonance in the photodetachment cross section, which fails to develop into the full Beutler-Fano profile before the onset of the threshold.

In the immediate neighborhood of the threshold, significant differences between the three- and four-state results for the photodetachment cross section occur (see Fig. 5). Although both calculations yield much the same shape, the four-state cross section is smaller by $(3-6)\times10^{-18}$ cm^2. In the region from 10×10^{-4} to 18×10^{-4} Ry below threshold the four-state result is also a little flatter. In the figure are also displayed the partial photodetachment cross sections for leaving the atom in its first excited state. Again the three-state approximation gives the slightly larger result.

Both the measures of convergence given in Tables III and IV and in Figs. 3 and 5, and the good agreement with measurements displayed in Figs. 3 and 4, suggest that the four-state calculations in LS coupling are converged to within a few percent, and therefore provide a reliable basis for the next stage of this work.

IV. MULTICHANNEL PHOTODETACHMENT THEORY

In this section we summarize the formulas[22] used to evaluate the cross section for photodetachment in the vicinity of $4\,^2P^o$ state of potassium, including the effect of fine-structure splitting. It is convenient to consider (3.1) as an element in the vector product[23]

$$\sigma=4\pi^2\alpha a_0^2\frac{h\nu}{\omega}[\vec{D}(\mathbf{S})]^\dagger\cdot\vec{D}(\mathbf{S}) \tag{4.1}$$

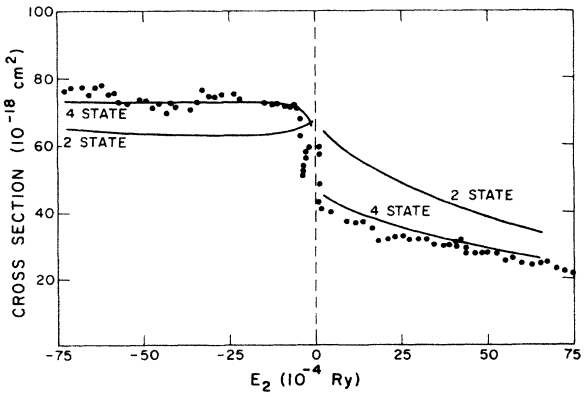

FIG. 4. As in Fig. 3 in the vicinity of the $4p\,^2P^o$ threshold (vs electron energy relative to this threshold) compared with the relative measurements of Ref. 6.

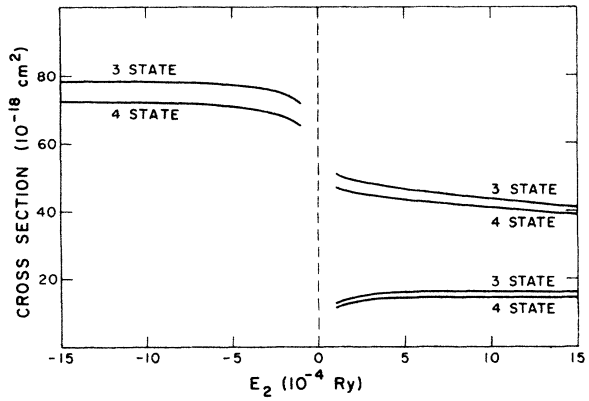

FIG. 5. Cross sections for photodetachment of K^- in the vicinity of the $4p\,^2P^o$ threshold in the three- and four-state approximations and in LS coupling: total cross sections, upper curves; cross sections for excited state channels only, lower curves.

for the total cross section. The vector of dipole matrix elements $\vec{D}(\mathbf{S})$ involves integrals over radial wave functions for the outgoing electron with scattering matrix (complex) boundary conditions corresponding to incoming waves in all channels and outgoing waves in only one channel.

A. Expressions analytic in the energy

For practical calculations, we use instead wave functions with reactance matrix (real) boundary conditions, and express $\vec{D}(\mathbf{S})$ as

$$\vec{D}(\mathbf{S})=(ik^{-(l+1/2)}+\mathbf{M}k^{l+1/2})^{-1}\vec{D}(\mathbf{M})\,, \tag{4.2}$$

where $\mathbf{M}$ and $\vec{D}(\mathbf{M})$ are real, and $k^{\pm(l+1/2)}$ are diagonal matrices of channel momenta. The matrix $\mathbf{M}$ is related to the reactance matrix $\mathbf{R}$ and the scattering matrix $\mathbf{S}$ by

$$\mathbf{M}=k^{-(l+1/2)}\mathbf{R}k^{-(l+1/2)} \tag{4.3}$$

and

$$\mathbf{S}=(1+i\mathbf{R})(1-i\mathbf{R})^{-1}\,. \tag{4.4}$$

The dipole matrix elements $\vec{D}(\mathbf{M})$ involve integrals over radial functions for the outgoing electron that have the asymptotic form

$$\mathbf{F}_{oo}(\mathbf{M},r)\underset{r\to\infty}{\sim}\left[\frac{2}{\pi}\right]^{1/2}[k^{-(l+1)}\sin(kr-l\pi/2)+k^l\cos(kr-l\pi/2)\mathbf{M}] \tag{4.5}$$

and

$$\mathbf{F}_{co}(\mathbf{M},r)\underset{r\to\infty}{\sim}0\,,$$

where oo and co designate the open- and closed-channel subsets of the wave function for all energetically accessible final states. The number of open channels thus determines the order of $\vec{D}(\mathbf{M})$ and $\mathbf{M}$.

For a potential of finite range, as seen by the outgoing electron, the more general functions $\mathscr{M}$ and $\vec{D}(\mathscr{M})$ are analytic in the energy and presumably slowly varying in the vicinity of a threshold. This property follows, however, only in the *absence* of the additional physical boundary condition imposed on $\mathbf{F}_{co}(\mathbf{M},r)$, i.e., mathematically the analytic function $\mathbf{F}_{co}(\mathscr{M},r)$ has growing exponential components. The expression relating $\mathbf{M}$ and $\mathscr{M}$ is

$$\mathbf{M}=\mathscr{M}_{oo}-\mathscr{M}_{oc}[(-1)^l\kappa^{-(2l+1)}+\mathscr{M}_{cc}]^{-1}\mathscr{M}_{co}\ , \tag{4.6}$$

where $\kappa\rightarrow i\kappa$ and $\kappa>0$ as an open channel becomes closed. The form (4.6) clearly allows for resonance behavior, i.e., rapid variation, in $\mathbf{M}$ even for constant $\mathscr{M}$. The expression corresponding to (4.6) for $\vec{D}(\mathbf{M})$ is

$$\vec{D}(\mathbf{M})=\vec{D}_o(\mathscr{M})-\mathscr{M}_{oc}[(-1)^l\kappa^{-(2l+1)}+\mathscr{M}_{cc}]^{-1}\vec{D}_c(\mathscr{M})\ . \tag{4.7}$$

Contact can be made with perhaps more familiar material by noting that for a single open channel and $l=0$, $\mathscr{M}=k^{-1}\tan\eta=-a$, where η is the scattering phase shift and a is referred to as the scattering length. Now if this single channel becomes closed, (4.5) has a pole for $\kappa=1/a$, i.e., there is a bound state near threshold for large positive a.

It is obvious that for all channels open we must have $\mathbf{M}=\mathscr{M}$ and $\vec{D}(\mathbf{M})=\vec{D}(\mathscr{M})$. Thus if $\mathscr{M}$ and $\vec{D}(\mathscr{M})$ may be presumed constants, all of the energy dependence in the elements $\vec{D}(\mathbf{S})$ is explicitly displayed in the factors of k and κ in (4.2), (4.6), and (4.7). For the case of only two channels, that appropriate to the present problem, the total and partial photodetachment cross section can be completely defined by specifying only five parameters ($\mathscr{M}_{11}$, $\mathscr{M}_{12}$, $\mathscr{M}_{22}$, D_1, and D_2).

B. Recoupling of angular momenta

The formalism to this point presumes no particular algebraic coupling scheme. If we are to introduce the effect of fine-structure splitting after the fact of calculations that are essentially nonrelativistic, i.e., in LS coupling, it is clear that a simple algebraic recoupling is involved followed by some phenomenological introduction of the finite energy splitting of the multiplet. The vehicles most appropriate for the algebraic transformation are obviously $\mathscr{M}$ and $\vec{D}(\mathscr{M})$, since these quantities are by definition constant or slowly varying in the vicinity of the threshold. Thus if $\mathbf{V}$ is the algebraic transformation such that

$$\vec{\Psi}^{\,jj}=\vec{\Psi}^{\,LS}\mathbf{V}\ , \tag{4.8}$$

then it follows that

$$\mathscr{M}^{jj}=\mathbf{V}^T\mathscr{M}^{LS}\mathbf{V} \tag{4.9}$$

and

$$\vec{D}^{\,jj}(\mathscr{M})=\mathbf{V}^T\vec{D}^{\,LS}(\mathscr{M})\ . \tag{4.10}$$

The quantities $\mathscr{M}^{jj}$ and $\vec{D}^{\,jj}(\mathscr{M})$ may then be used in (4.6) and (4.7), and the results in (4.2), with all the channel momenta in these equations redefined so as to reflect the physical fine-structure splitting.

C. Alternative boundary conditions

A completely equivalent set of expressions can be developed by imposing a much more general set of boundary conditions than implied by (4.5), viz.,

$$\mathbf{F}(\mathscr{M}')\underset{r\rightarrow\infty}{\sim}\left[\frac{2}{\pi}\right]^{1/2}[k^{-(l+1)}\sin(kr+\rho-l\pi/2)+k^l\cos(kr+\rho-l\pi/2)\mathscr{M}']\ . \tag{4.11}$$

With minimal constraints on ρ it follows that $\mathscr{M}'$ is also an analytic function of the energy.

The generalizations of (4.2), (4.6), and (4.7) are

$$\vec{D}(\mathbf{S})=e^{i\rho}(ik^{-(l+1/2)}+\mathbf{M}'k^{l+1/2})^{-1}\vec{D}(\mathbf{M}')\ , \tag{4.12}$$

$$\mathbf{M}'=\mathscr{M}'_{oo}-\mathscr{M}'_{oc}[(-1)^l\kappa^{-(2l+1)}+\mathscr{M}'_{cc}]^{-1}\mathscr{M}'_{co}\ , \tag{4.13}$$

and

$$\vec{D}(\mathbf{M}')=\vec{D}_o(\mathscr{M}')-\mathscr{M}'_{oc}[(-1)^l\kappa^{-(2l+1)}+\mathscr{M}'_{cc}]\vec{D}_c(\mathscr{M}')\ . \tag{4.14}$$

It is obvious that the resulting partial and total cross sections defined by (4.12) must be independent of ρ. We also see that the *form* of the expression (4.1) for the cross sections themselves is invariant, i.e., depends only implicitly on ρ. The relationship between $\mathscr{M}'$ and $\mathscr{M}$ and between $\vec{D}(\mathscr{M}')$ and $\vec{D}(\mathscr{M})$, are

$$\mathscr{M}'=(\cos\rho+\mathscr{M}k^{2l+1}\sin\rho)^{-1}(-k^{-(2l+1)}\sin\rho+\mathscr{M}\cos\rho) \tag{4.15}$$

and

$$\vec{D}(\mathscr{M}')=(\cos\rho+\mathscr{M}k^{2l+1}\sin\rho)^{-1}\vec{D}(\mathscr{M})\ . \tag{4.16}$$

Uses or interpretations of ρ are several. For potentials of finite range, $\mathscr{M}$ may have simple poles and ρ may be chosen so as to render $\mathscr{M}'$ slowly varying. For long-range potentials, such as in the present case, ρ might be chosen so as to subsume the dominant effect of the long-range interaction, thereby yielding slowly varying quantities $\mathscr{M}'$ and $\vec{D}(\mathscr{M}')$ from more rapidly varying $\mathscr{M}$ and $\vec{D}(\mathscr{M})$. [Here complete rigor is not possible, since in the presence of long-range potentials $\mathscr{M}$ and $\vec{D}(\mathscr{M})$ are not strictly analytic functions, but as a practical matter it may still be possible to treat them as such.] This done, (4.9) and (4.10) may be applied to $\mathscr{M}'$ and $\vec{D}(\mathscr{M}')$, and (4.1) with (4.12)–(4.14) used to calculate the photodetachment cross sections with no further reference to ρ.

V. ANALYSIS OF CALCULATIONS

A. The reactance and dipole matrix elements

In this analysis of the reactance matrix elements characterizing the $^1P^o$ and $^3P^o$ partial-wave contributions

to the $K+e$ collision problem and the corresponding dipole matrix elements linking the initial bound K^- wave function to the final free $K+e$ wave functions in $^1P^o$ symmetry, considerable use has been made of the transformation theory summarized in Sec. IV.

As they emerge from the computer codes,[9] the wave functions and reactance matrix elements are consistent with the conventional (real, reactance matrix) boundary conditions. Each reactance matrix **R** was first written in the form $\mathscr{M}$ using (4.3). The elements of these matrices which involve the electron going out as a d wave are then neglected, since in the threshold region of interest the corresponding partial photodetachment cross section was found to be smaller than the others by 2 orders of magnitude. Thus at each energy point above the $^2P^o$ threshold we are left with a 2×2 matrix $\mathscr{M}^{LS}$ for each of the $^1P^o$ and $^3P^o$ symmetries. Since each matrix is symmetric it has three independent elements. There are also two independent analytic dipole matrix elements D_1 and D_2 corresponding to the two possible exit channels for the detached electron at these energies.

All these matrix elements are then subjected to energy-dependent transformations (4.15) and (4.16), yielding new matrices $\mathscr{M}'$ and vectors $\vec{D}(\mathscr{M}')$. The actual transformations used had zero phase angle in the ground-state channel, i.e., $\rho_1=0$, and rotation proportional to k in the excited-state channel, i.e., $\rho_2=\gamma k_2$. Of course, through the nonzero off-diagonal matrix elements, all the matrix elements alter under such a transformation. A set of such transformations is produced by choosing different values of γ.

The results of some of this set of transformations on the various four-state matrix elements are displayed in Fig. 6. The untransformed $^1P^o$ elements (corresponding to $\gamma=0$) can all be seen to vary extremely rapidly in the narrow energy band above threshold. This rapid variation is reduced as transformations corresponding to increasingly negative values of γ are chosen. On the other hand, the transformed $^3P^o$ elements, although initially varying less rapidly as γ is made negative soon show very marked variation as γ is made still more negative.

As noted in Sec. IV C, the same cross section is produced by the set of transformed elements provided these are all the result of the same transformation. It also follows from the form of (4.9), (4.10), and (4.12) that the photodetachment cross sections obtained after an algebraic transformation to jj coupling remain independent of the transformations if *all* matrix elements involved have been subjected to the *same* transformation. For instance, in our example it would be incorrect to mix $^1P^o$ matrix elements transformed by $\rho_1=0$, $\rho_2=-6k_2$ with $^3P^o$ matrix elements transformed by $\rho_1=0$, $\rho_2=-3k_2$.

Our aim is to produce a photodetachment cross section taking the fine-structure splitting of the $^2P^o$ state into account. Hence we have an interest only in transformations that make both $^1P^o$ and $^3P^o$ matrix elements reasonably constant and hence easily extrapolated in the threshold region. Bearing in mind that the transformation for the $^1P^o$ elements must be the same as that for the $^3P^o$ elements, it appears $\rho_1=0$, $\rho_2=-18.0k_2$ is a good compromise to obtain fairly constant transformed elements from the four-state calculation. It turns out this is a good choice also for the three-state numbers.

That such a simple transformation produces results for both $\mathscr{M}$ and $\vec{D}(\mathscr{M})$ that are remarkably constant, without recourse to additional fitting parameters, is not fortuitous. In rigorous treatments[12,24] of the long-range polarization force, there are two other parameters required in addition to the phase shift. Only if these two additional parameters are quasiconstants will a single phase shift suffice. In the formal treatment[21] based on Mathieu functions, this is decidely not the case, owing to the singular form adopted for the potential at the origin. In the numerical treatment by Oppenheimer-Berger *et al.*,[24] however, the polarization potential is subjected to a physically motivated cutoff for small distances, and there is a cutoff for which the two additional parameters are slowly varying. This is the parameter set for $\beta/d\sim2.6$, where $\beta^2=\alpha$ is the polarizability and d is the radius, in a.u.; for $\alpha=604$ a.u., $\beta\sim25$ and hence d is $\sim10a_0$, a quite reasonable value for potassium. The numerically calculated[24] phase shift for this cutoff is quite close to the value that we obtained by fitting. The chosen phase rotation, therefore, has in fact subsumed the dominant effect of the long-range polarization force.

The question remains as how best to extrapolate the chosen set of transformed matrix elements below the threshold. This is necessary since the close-coupling calculations do not yield the complete untransformed elements in this region but rather the physical elements derived from them, i.e., the left-hand side of (4.6) and (4.7). The complete set $\mathscr{M}'$ and $\vec{D}(\mathscr{M}')$ is required in the algebraic transformation to jj coupling.

It was found best to perform this extrapolation by means of parabolas defined by requiring that each pass through the values taken by a given element at 1×10^{-4}, 4×10^{-4}, and 7×10^{-4} Ry above threshold (the fine-structure splitting of the $4\,^2P^o$ state is $\sim5\times10^{-4}$ Ry). The coefficients of the parabolic fits for both the three- and four-state elements are given in Tables V and VI. As an indication of the goodness of this quadratic fit for, specifically, the $^1P^o$ elements, we show in Fig. 7 the photodetachment cross section calculated in the immediate neighborhood of the $^2P^o$ threshold in LS coupling using the quadratic fits to the four-state transformed elements compared with the actual results from the original four-state calculation. Also included on the figure are the positions of $^2P_{1/2,3/2}$ thresholds. Significant differences appear only at those energies at substantial distances from threshold compared to the size of the fine-structure splitting and hence outside our range of interest.

B. The photodetachment cross section in jj coupling

Using the quadratic form representation of the transformed matrix elements discussed above, the photodetachment cross section was calculated in a jj coupling scheme over the region of the fine-structure splitting of the $^2P^o$ state. The algebraic coefficients used in (4.9) and (4.10) are given by Lee.[13]

The jj-coupling cross sections from this analysis of the

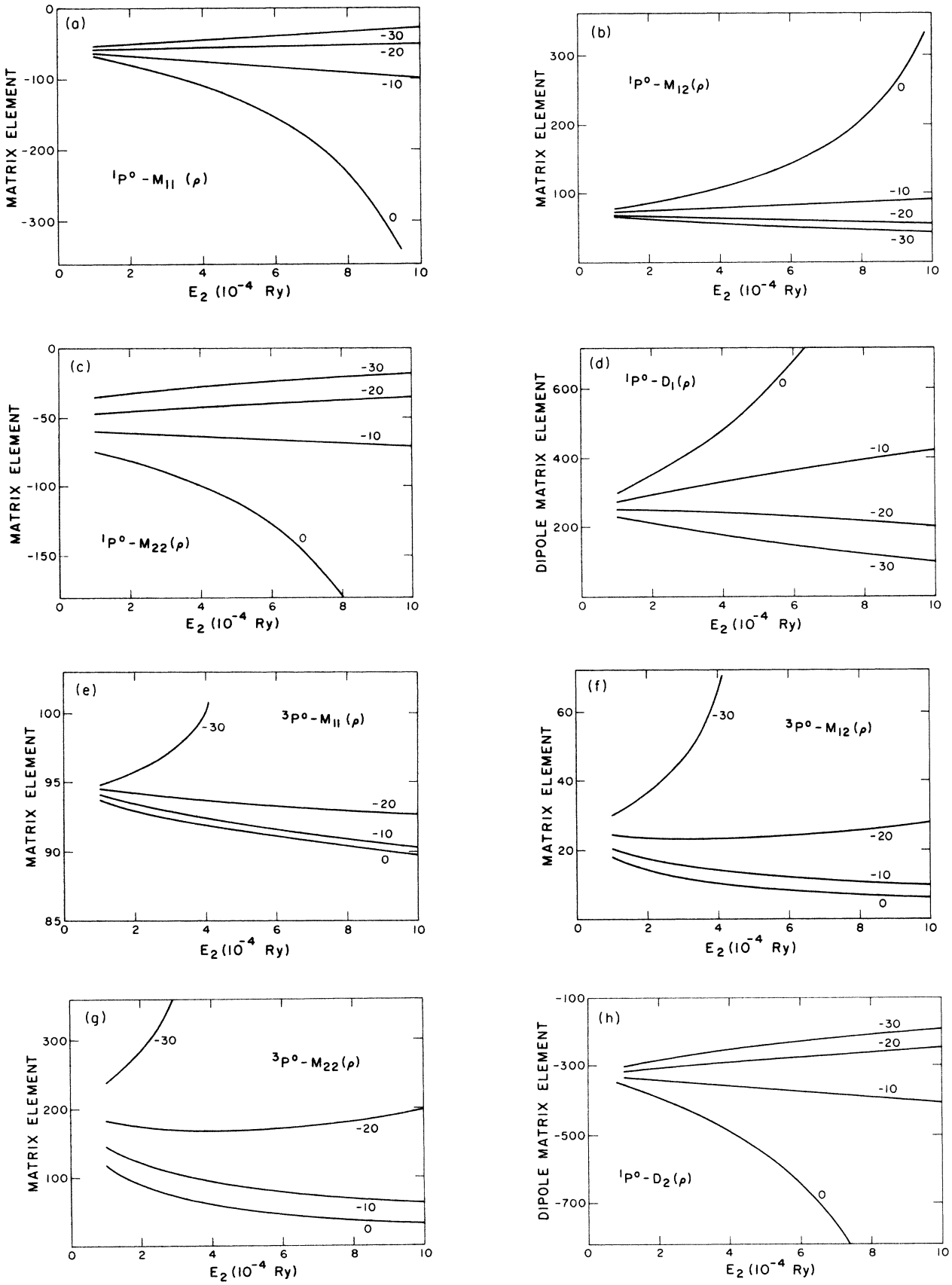

FIG. 6. Illustrative results for the effect of phase transformations on the elements of the reactance matrices ($\mathcal{M}_{ij}$) and dipole matrix elements (D_i) as a function of the constant γ in the phase $\rho=\gamma k_2$, vs electron energy relative to the $4p\,^2P^o$ threshold: (a) $^1P^o$, $\mathcal{M}_{11}$; (b) $^1P^o$, $\mathcal{M}_{12}$; (c) $^1P^o$, $\mathcal{M}_{22}$; (d) D_1; (e) $^3P^o$, $\mathcal{M}_{11}$; (f) $^3P^o$, $\mathcal{M}_{12}$; (g) $^3P^o$, $\mathcal{M}_{22}$; (h) D_2.

TABLE V. Coefficients of the quadratic fit ax^2+bx+c to the reduced (M) and dipole (D) matrix elements for the three-state results; x is the $4p$ channel energy in 10^{-4} Ry.

		a	b	c
$^1P^o$	M_{11}	0.094 44	−0.438 89	−55.755 56
	M_{12}	0.005 55	−1.161 11	69.055 56
	M_{22}	0.0	1.100 00	−51.400 00
	D_1	0.444 44	−1.222 22	−260.222 22
	D_2	0.0	−6.333 33	331.333 33
$^3P^o$	M_{11}	0.016 67	−0.416 67	91.400 00
	M_{12}	0.050 00	−0.650 00	19.100 00
	M_{22}	0.272 22	−3.994 44	69.322 22

three- and four-state calculations are shown in Figs. 8 and 9. Also included in these figures are dots representing the experimental results of Slater *et al.*[4] for the total photodetachment cross section and for the partial cross section corresponding to the detachment of a slow electron leaving the atom in either fine-structure level of its first excited $^2P^o$ state. Neither experimental measurement is absolute and so, for comparison purposes, in each figure the total measured photodetachment cross section has been normalized to the calculated quantity at an energy below the $^2P_{1/2}$ threshold and the measured partial cross section normalized to the same calculated quantity at an energy above the $^2P_{3/2}$ threshold.

It is clear the four-state calculation yields both total and partial photodetachment cross sections in better agreement with the experimental results than does the three-state calculation. Nevertheless, an interesting feature, namely the sharp dip in the total cross section at the $^2P_{1/2}$ threshold, is still not sharp enough in the four-state calculation. The experimental total cross-section measurement also falls off much more rapidly at the $^2P_{3/2}$ threshold than is indicated by either calculation.

Considering the trend toward better agreement with experiment we looked to see how corresponding matrix elements from the two calculations differed. Examining the quadratic fits to the transformed elements—a meaningful comparison since both three- and four-state numbers have been obtained by exactly the same rotation—it is clear the main difference is in the $\mathscr{M}'_{22}$ element for $^3P^o$. The three-state calculation gives 69.32 as the leading constant term while the four-state calculation gives 189.0. The magnitude of this term is governed by the distance of the virtual state in $^3P^o$ symmetry from the $^2P^o$ threshold. It is plausible as discussed in Sec. III B to assume that the converged position of this state is closer to threshold than obtained even in the four-state calculation.

TABLE VI. As Table V, for the four-state results.

		a	b	c
$^2P^o$	M_{11}	0.122 22	−0.877 78	−57.044 44
	M_{12}	0.0	−1.133 33	70.833 33
	M_{22}	0.005 56	1.038 89	−50.144 44
	D_1	−0.611 11	3.388 89	252.222 22
	D_2	0.0	6.000 00	−324.000 00
$^3P^o$	M_{11}	0.011 11	−0.422 22	94.811 11
	M_{12}	0.122 22	−1.577 78	24.855 56
	M_{22}	1.166 67	−15.166 67	189.000 00

TABLE VII. Comparison of the polarization-based parameters obtained from the present results and from fitting to experimental data. The eigenvalues μ_1,μ_2 and the mixing angle θ_1 refer to $^1P^o$ scattering; μ_3, μ_4, and θ_3 to $^3P^o$ scattering.

	Calculated[a]	Measured[b]
θ_1	0.254	0.238
θ_3	−0.007	−0.048
$\tan(\pi\mu_1)$	20.68	19.55
$\tan(\pi\mu_2)$	−1.00	−0.760
$\tan(\pi\mu_3)$	90.11	-1×10^4
$\tan(\pi\mu_4)$	−0.135	−0.046
D_1^P/D_2^P	−4.08	−4.78

[a]Reference 12.
[b]Reference 7.

Accordingly, the four-state calculation was repeated except the value of 189.0 for the leading term in the quadratic representation of the $^3P^o$ $\mathscr{M}'_{22}$ element was replaced by the value of 500.0. The total and partial photodetachment cross sections given in Fig. 10 are the result. The effect was to make the shape of partial cross section in excellent agreement with experiment. Also the dip in the total cross section near the $^2P_{1/2}$ threshold is deepened and in improved agreement with experiment.

The effect of the change in this $^3P^o$ element on the eigenphases of the jj-coupled reactance matrix over the threshold region is displayed in Fig. 11. Most of the eigenphases remain unchanged but the one starting up from zero at the $^2P_{1/2}$ threshold climbs much more rapidly in the adjusted four-state calculation than in the unaltered calculation.

The adjustment of the $^3P^o$ $\mathscr{M}'_{22}$ element had little effect on the shape of the total cross section near the $^2P_{3/2}$

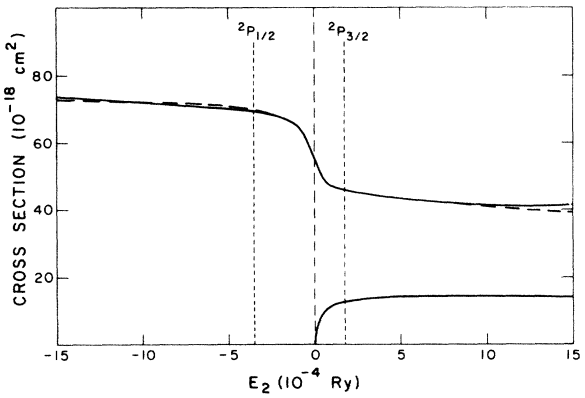

FIG. 7. Cross sections for photodetachment of K^- in the vicinity of the $4p$ $^2P^o$ threshold from the four-state calculations (— — —), and obtained using the quadratic fit to the transformed reactance and dipole matrix elements from that calculation (——): total cross section, upper curves; cross sections for excited-state channels only, lower curves (directly calculated and fit curves indistinguishable).

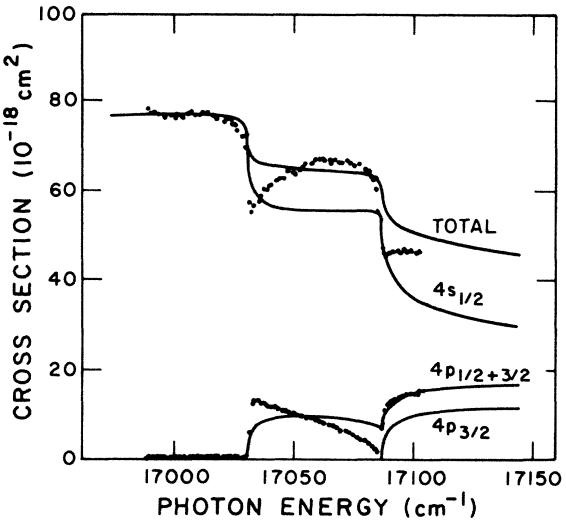

FIG. 8. Cross sections for photodetachment of K^- in the vicinity of the $4p_{1/2}$ and $4p_{3/2}$ thresholds from the three-state calculations, as a function of photon energy, compared with the relative measurements of Ref. 4; labels indicate the final state of the potassium atom.

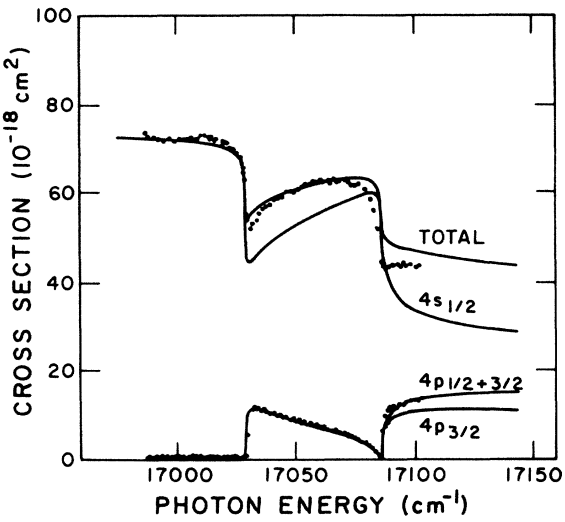

FIG. 10. As in Fig. 9, but with the leading term of the quadratic representation of $M_{22}(^3P^o)$ increased to improve the fit with the measurements.

threshold. Since the four-state calculation result differs little from the three-state calculation in this region it is unreasonable to expect an extrapolation of any trend in going from one to the other to produce much change. Some experimentation was tried to find out how sensitive the cross sections are to variations in magnitude and sign of the elements. It was found that the total cross section was sensitive to the ratio of the dipole matrix elements. In Fig. 12 we show the effect of reducing the magnitude of the leading constant term in the quadratic representation of $D_1(\mathcal{M}')$ to 233.5 and retaining 500.0 as the value of the leading constant term in the $^3P^o$ $\mathcal{M}'_{22}$ element. The agreement of the total cross section with the experiment in the neighborhood of the $^2P_{3/2}$ threshold and between the thresholds is, with this change of less than 9% in the ratio D_1 to D_2, greatly improved to only the slight detriment of agreement below the $^2P_{1/2}$ threshold.

In their analysis, Watanabe and Greene[12] started with our values for the $^3P^o$ and $^1P^o$ $\mathcal{M}$ matrices and associated dipole vector $\vec{D}(\mathcal{M})$ at 5×10^{-4} Ry above the $^2P^o$ threshold. At this energy point [using the inverse of Eq. (3.6b) in their paper] they transformed these quantities into equivalent quantities with respect to Mathieu's solutions of the radial equation for the excited state channel containing a potential term α/r^4. They confirmed the presumption that these new quantities described the threshold region by transforming them back into the form of our $\mathcal{M}$ and $\vec{D}(\mathcal{M})$ at various energies in this range and comparing with our values for these quantities. In the

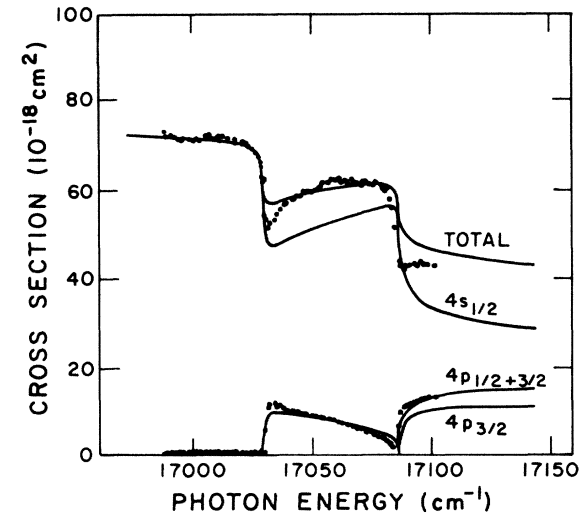

FIG. 9. As in Fig. 8 for the results of the four-state calculations.

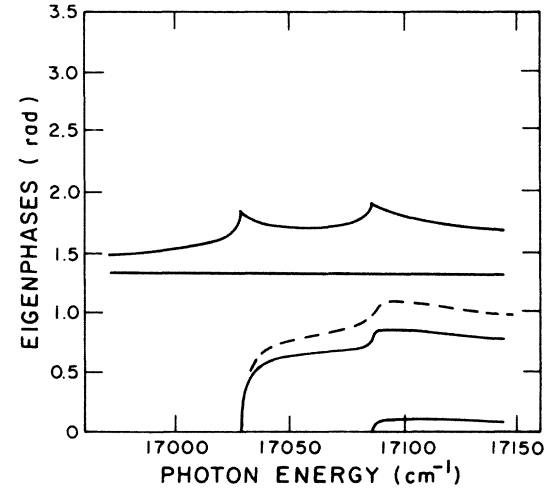

FIG. 11. Eigenphases for electron-potassium scattering in the vicinity of the $4p_{1/2}$ and $4p_{3/2}$ thresholds for the four-state calculation (——), and with only the leading term of the quadratic representation of $M_{22}(^3P^o)$ increased (— — —).

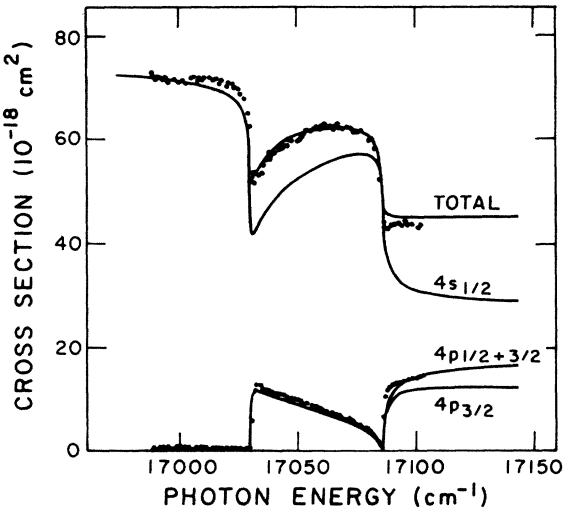

FIG. 12. As in Fig. 10, with the ratio of the leading terms in the quadratic representation of the dipole matrix elements also changed to improve the fit with the measurements.

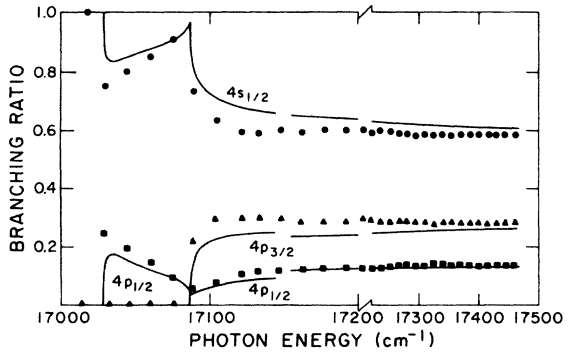

FIG. 13. Branching ratios for photodetachment of K^- to the $4s_{1/2}$, $4p_{1/2}$, and $4p_{3/2}$ states of potassium from the four-state calculations compared with the absolute measurements of Rouze and Geballe (Ref. 7).

case of the $\mathcal{M}$ matrices, this comparison was made through quantities related to the eigenvalues and eigenvectors of these matrices (see Figs. 5—7 of their paper). Although no attempt was made in their work to obtain a comparison with the experimental cross section over the fine-structure split threshold region they remark that the total and partial cross sections in *LS* coupling (i.e., from the $^1P^o$ quantities) appear identical to ours.

This question of comparison of results arising from this formulation of the problem with experimental data was taken up by Rouze and Geballe.[7] They fit the total and combined $^2P_{1/2}$ and $^2P_{3/2}$ cross section data of Slater *et al.*[4] to obtain values of the Watanabe and Greene parameters, and used these parameters to produce branching ratios for comparison with the results of their own measurements. It is interesting to compare these values with those Watanabe and Green obtained from our calculation; both sets are listed in Table VII. There are two points to which we would like to draw particular attention. Firstly, the Rouze and Geballe value for $\tan(\pi\mu_3)$ has a larger magnitude than the calculated quantity. This increase is in accord with the progression from Fig. 9 to Fig. 10, in which we justified increasing the value of our $^3P^o$ $\mathcal{M}'_{22}$ matrix element on physical grounds and gained improved agreement with experiment. Secondly, the Rouze and Geballe value for D_1^P/D_2^P has again a larger magnitude than the calculated quantity. This is, in fact, completely consistent with the change we found necessary in order to obtain the extremely satisfactory agreement with experiment displayed in Fig. 12.

We also note in passing that our calculation agrees with the relative magnitude of partial to total cross sections found by Rouze and Geballe and supports their suggestion that the Slater *et al.* value for the partial cross section for leaving the atom in the $4p\,^2P^o$ states should be multiplied by about 0.8 with respect to their total cross-section curve. Our results are compared with those of Rouze and Geballe in Fig. 13. The calculated results shown are those consistent with Fig. 9, i.e., without any subsequent *ad hoc* adjustment of the parameters. It is clear, however, that if the cross sections given in Fig. 12 were used instead, the agreement would be substantially improved.

ACKNOWLEDGMENTS

This work was supported by National Science Foundation Grant No. PHY82-00805 through the University of Colorado. The authors thank T. A. Patterson, H. Hotop, and W. C. Lineberger for supplying unpublished data.

*Present address: Department of Mathematics, Royal Holloway and Bedford New College, University of London, Egham Hill, Egham, Surrey, TW20 0EX England.

†Quantum Physics Division, National Bureau of Standards.

[1]E. P. Wigner, Phys. Rev. 73, 1002 (1948).

[2]See, for a general discussion of photodetachment threshold laws, R. D. Mead, K. R. Lykke, and W. C. Lineberger, in *Electronic and Atomic Collisions,* edited by J. Eichler, I. V. Hertel, and N. Stolterfoht (North-Holland, Amsterdam, 1984), p. 721.

[3]T. A. Patterson, H. Hotop, A. Kasdan, D. W. Norcross, and W. C. Lineberger, Phys. Rev. Lett. 32, 189 (1974).

[4]J. Slater, F. H. Read, S. E. Novick, and W. C. Lineberger, Phys. Rev. A 17, 201 (1978).

[5]H. J. Kaiser, E. Heinicke, R. Rackwitz, and D. Feldman, Z. Phys. 270, 259 (1974).

[6]T. A. Patterson, H. Hotop, and W. C. Lineberger (private communication).

[7]R. A. Falk, D. Leep, and R. Geballe, Phys. Rev. A 22, 1099 (1980); N. Rouze and R. Geballe, *ibid.* 27, 3071 (1983).

[8]D. L. Moores and D. W. Norcross, Phys. Rev. A 10, 1646 (1974).

[9]M. A. Crees, M. J. Seaton, and P. M. H. Wilson, Comput. Phys. Commun. **15**, 23 (1978); W. Eissner and M. J. Seaton, J. Phys. B **5**, 2187 (1972); H. Saraph (private communication).
[10]M. H. Ross and G. L. Shaw, Ann. Phys. (N.Y.) **9**, 391 (1960).
[11]M. J. Seaton, Rep. Prog. Phys. **46**, 167 (1983); J. Dubau and M. J. Seaton, J. Phys. B **17**, 381 (1984).
[12]S. Watanabe and C. H. Greene, Phys. Rev. A **22**, 158 (1980).
[13]C. M. Lee, Phys. Rev. A **11**, 1692 (1975).
[14]R. Risberg, Ark. Fys. **10**, 583 (1956).
[15]G. Stephenson, Proc. Phys. Soc. London **64**, 458 (1951); Yu. I. Ostrovski and N. P. Penkin, Opt. Spekstrosk. **12**, 669 (1962) [Opt. Spectrosc. **12**, 379 (1962)]; J. K. Link, J. Opt. Soc. Am. **56**, 1195 (1966); R. W. Schmieder, A. Lurio, and W. Happer, Phys. Rev. **173**, 76 (1968); G. Copley and L. Krause, Can. J. Phys. **47**, 533 (1969); D. Zimmermann, Z. Phys. **275**, 5 (1975).
[16]D. S. Villars, J. Opt. Soc. Am. **42**, 552 (1952).
[17]U. Teppner and P. Zimmermann, Astron. Astrophys. **64**, 215 (1978).
[18]See, for example, D. W. Norcross, Phys. Rev. A **7**, 606 (1973).
[19]R. W. Molof, H. L. Schwartz, T. M. Miller, and B. Bederson, Phys. Rev. **10**, 1131 (1974).
[20]W. L. Wiese, M. W. Smith, and B. M. Miles, *Atomic Transition Probabilites,* Natl. Bur. Stand. Ref. Data Ser., Natl. Bur. Stand (U.S.) Circ. No. 4 (U.S. GPO, Washington, D.C., 1969), Vol. II, p. 225.
[21]D. W. Norcross and M. J. Seaton, J. Phys. B **6**, 614 (1973).
[22]D. W. Norcross and K. T. Taylor (unpublished).
[23]Matrices are indicated by bold notation.
[24]R. O.-Berger, H. B. Snodgrass, and L. Spruch, Phys. Rev. **185**, 113 (1969).